Motion Control via Muscle Synergies: Application to Throwing

Ana Lucia Cruz Ruiz, Charles Pontonnier, Jonathan Levy, Georges Dumont

Motion Control via Muscle Synergies: Application to Throwing

Ana Lucia Cruz Ruiz*
INRIA/IRISA, Rennes, France
Ecole Normale Supérieure de Rennes, Bruz, France

Charles Pontonnier
IRISA/INRIA, Rennes, France
Ecoles de Saint-Cyr Coëtquidan, Guer, France
Ecole Normale Supérieure de Rennes, Bruz, France

Jonathan Levy
Ecole Normale Supérieure de Rennes, Bruz, France

Georges Dumont
Ecole Normale Supérieure de Rennes, Bruz, France
IRISA/INRIA, Rennes, France

Abstract

In the current paper, we present a control method based on muscle synergy extraction and adaptation to drive a human arm in a direct dynamics simulation of an overhead throwing motion. The experimental protocol for synergy extraction and model are first presented, followed by a control method consisting of a series of optimizations to adapt muscle parameters and synergies to match experimental data. Results show that the motion can be accurately reproduced thanks to the muscle synergy extraction and adaptation to the model.

CR Categories: I.3.7 [Computer Graphics]: Three-Dimensional Graphics and Realism—Animation

Keywords: motion synthesis, physical simulation, optimization, musculoskeletal model

1 Introduction

Synthesizing new motions by only specifying task-space goals is really appealing, especially for the game industry, where it is important to grant characters with the possibility of a rich motion diversity in relation to the current game state. In fact, even if synthesising new motions from captured motions is feasible [Kulpa et al. 2005; Pronost and Dumont 2007], it is still limited by the available motion database. For example, it has recently been shown that motion capture edition and warping have strong perceptual limits for throwing motions, meaning that they are not perceived natural enough by users [Vicovaro et al. 2014].

Physically-based motion synthesis is a promising field, especially to synthesize realistic motions from scratch [Geijtenbeek and Pronost 2012]. However, physically-based approaches have been strongly hampered by the modelling of the actuation. Torque-driven simulations have often being characterized as robot-like and unnatural [Hodgins and Wooten 1998], despite of strong improvements in motion control [Yin et al. 2007].

Therefore, one of the key issues of achieving natural motions is the actuation modelling. Adding the muscle layer on the skeletal representation of the human has several advantages. First of all, muscles can be considered as visco-elastic actuators [Hill 1938], giving a natural smoothness to the motion [Geyer and Herr 2010]. Second, the passive elements of the muscular complex (tendons, ligaments) provide a natural stability to the system [Gerritsen et al. 1995]. These advantages have begun to inspire animators, resulting in partially or entirely muscle actuated characters. For instance, [Wang et al. 2012] incorporated muscles to the lower body of a humanoid character, and evidenced through visual, kinematic and dynamic comparisons, that walking and running motions synthesized via energy estimates that used muscles, were closer to real human data than those that used torques. [Mordatch et al. 2013] also used a humanoid with muscles in the lower body and synthesized more challenging motions such as jumping and kicking.
Few authors have actuated virtual characters entirely by muscles. However, some recent examples featured musculoskeletal models in tasks such as locomotion [Geijtenbeek et al. 2013] and swimming [Si et al. 2014]. The former approach showed the increased visual realism of such motions thanks to the presence of certain properties of muscles, such as activation delays. The latter evidenced that torque based simulations also yielded plausible results at the expense of smaller simulation steps and higher control gains. Finally, other approaches have employed muscles as a natural solution to make motions more adaptable. [Lee et al. 2014] synthesized new gaits by adapting biped gaits to conditions such as muscle weakness, joint dislocation, tightness, pain reduction and maximization of efficiency.

However, muscle-driven avatars still present strong challenges. First of all, the human body exhibits more muscles than functional degrees of freedom, meaning that an infinity of solutions can be found to the forward dynamics problem yielding the proper muscle forces to achieve a specified motion [Erdemir et al. 2007]. Second, muscles are non linear visco-elastic actuators, meaning that their action cannot be handled by classical linear control theory [Cruz Ruiz et al. 2014]. Muscles can also have multiple actions, meaning that they can actuate several degrees of freedom with different degrees of contribution [Erdemir et al. 2007]. Finally, driving an avatar with muscles can be summarized as a non-linear and over actuated control problem. A solution to solve such a problem can lie in the reduction of the number of control variables, thanks to hypotheses about the way the Central Nervous System (CNS) controls the motion, such as the muscle synergy theory. This theory states that task level commands are translated into a reduced number of modules or synergies, which are later mapped into a larger set of individual muscle activations. Consequently this compact and reduced representation has the potential to produce a more efficient control of musculoskeletal models.

We propose a control method for avatar animation based on the muscle synergy theory. Muscle synergies, extracted from experimental data and adapted to the model are used to drive a forward dynamics simulation of an overhead throwing motion. We first present the experimental protocol, the human model and the muscles associated, followed by the control and the optimization methods that enable: i) an adaptation of the muscle parameters thanks to the experimental data ii) an adaptation of the synergy signals to match the experimental data. Results are presented for 3 degrees of freedom of an arm: shoulder, elbow and wrist, flexion and extension.

*e-mail:ana-lucia.cruz-ruiz@inria.fr

2 Material and Methods

2.1 Time-invariant synergy definition

Muscle synergies are defined as patterns of coordinated activations applied to a group of muscles [Alessandro et al. 2013; d'Avella and Lacquaniti 2013]. The muscle synergy hypothesis assumes that the CNS predefines a set of synergies, and combines them in a task-dependent manner to generate the proper muscle activations that produce a specified motion. In a general way, synergies are less numerous than the number of muscles actuated. Time-invariant or synchronous muscle synergies are one of the ways neuroscientists represent synergies. This was the model adopted in this study and the following paragraph presents it in detail.

A synchronous synergy w_i is defined as a D-dimensional vector of coefficients, specifying the relative activation level of D-muscles. Each synergy is paired with a time-varying combination coefficient vector $c_i(t)$, which determines its temporal evolution. A set of N-synergies can be linearly combined to generate D-muscle activation patterns $A(t)$:

$$A(t) = WC(t) = \sum_{i=1}^{N} w_i c_i(t) \tag{1}$$

Where, $A(t)$ is the $D \times T$ samples matrix containing the recorded muscle activations patterns, W is the $D \times N$ muscle synergy matrix, and $C(t)$ is the $N \times T$ samples combination coefficient matrix.

2.2 Data collection and synergy extraction

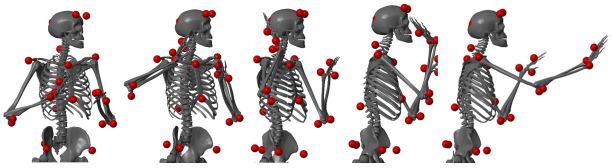

Figure 1: *Overhead throw to 2m target*

The protocol used for data collection and synergy extraction has been partially presented in [Cruz Ruiz et al. 2015]. Data was collected from overhead football throws to 2m, 4m and 7m targets (a description of this motion is featured in Figure 1). During this action, the muscle activation patterns for 10 right arm muscles were collected from a healthy 32-year old male (stature 1.86m, weight 72 kg), using surface electrodes (Cometa Waveplus EMG system, 1000Hz sampling rate) and well known electrode placement standards [Hermens et al. 1999]. These muscles were: the deltoids, the biceps, the triceps and the wrist extensors and flexors, which were recorded as a group. The EMG processing was made by following well known processing protocols [Konrad 2005]. The EMGs were amplified (gain 1000), digitized (1kHz), band-pass filtered (10-450Hz), rectified, and low-pass filtered (6Hz). ECG artifacts were removed using an ICA-based filtering procedure [Willigenburg et al. 2012]. Motion was captured with a Vicon system (15 cameras, 100Hz sampling rate).

Next, a NMF (Non-negative matrix factorization) algorithm [Kim and Park 2008] was used to extract a set of synchronous muscle synergies (section 2.1) and their corresponding combination coefficients from the recorded EMG pattern matrix $A(t)$ (this matrix was constructed by concatenating the EMG data for a total of 22 throws).

Essentially, NMF decomposes a non-negative matrix into a non-negative linear combination of basis vectors, by solving the following optimization problem:

$$\begin{aligned} \underset{W,C}{\text{minimize}} \quad & \frac{1}{2}||A(t) - WC(t)||_F^2 \\ \text{subject to} \quad & W, C(t) \geq 0 \end{aligned} \tag{2}$$

In order to reduce actuation redundancy, the number of synergies ($N = 5$) was chosen to be less than the number of muscles ($D = 6$) in the model described in the next section. Furthermore, although the extraction was made from 10 muscles, only the part of the synergies corresponding to the muscles in the model was considered. The extracted synergies and their time-varying combination coefficients are presented in section 3.1.

2.3 Character model

The character used in this study was developed in MATLAB® SimMechanics. It consists of a full body skeletal model with a musculoskeletal arm (Figure 2). The arm is actuated by six muscles (with actions on the sagittal plane) which are known to have important contributions in the task of throwing. The following sections detail further the skeletal model and its actuation.

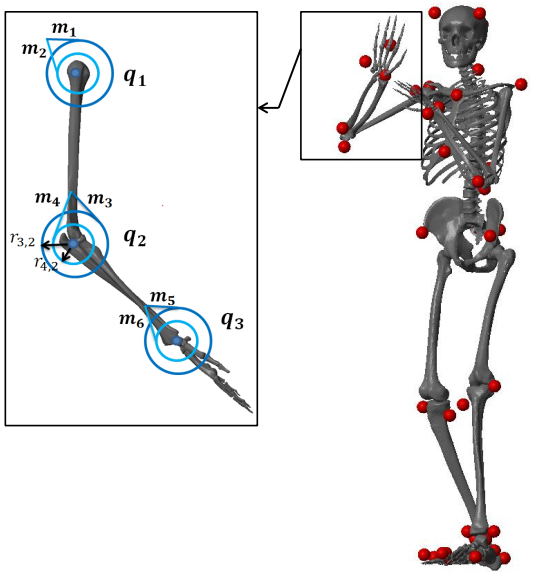

Figure 2: *Full body skeletal model and musculoskeletal arm model*

2.3.1 Skeletal model

The full body skeletal model consists of 21 rigid bodies linked by 17 joints, and exhibits 32 degrees of freedom. The method used to describe the skeletal model is based on a systematic structural representation. Except for the root (pelvis), each segment integrates a joint and its adjoined body. Thus, the segment representation does not depend on the other segments connected to it. This structural representation is described according to a hierarchical tree. From the root, each solid owns one child and one sister. A library containing several body part models issued from the literature, which can correspond to a segment or a set of segments, was used to build the model [Muller et al. 2015b]. The model used in the current study consists of well known and validated biomechanical models of the

spine [De Zee et al. 2007], the lower limbs [Horsman et al. 2007] and the upper limbs [Holzbaur et al. 2005].

The joints coordinates were estimated from motion capture, with an inverse kinematics method allowing the segment lengths and marker positions to be calibrated [Muller et al. 2015a]. Furthermore, Standard Body Segment Inertial Parameters (BSIP) were estimated using a scaling rule [Dumas et al. 2007].

2.3.2 Musculoskeletal arm model

The arm contains 3 degrees of freedom at the shoulder, 2 at the elbow and 2 at the wrist. The muscle-actuated degrees of freedom are the shoulder, elbow and wrist flexion (positive motion) and extension (negative motion). The remaining degrees of freedom of the arm are kinematically driven.

For simplicity, pairs of antagonistic muscle models [Rengifo et al. 2010] were used in order to reflect the action of real muscles on the segments. Figure 2 features a view of the musculoskeletal arm from the sagittal plane. The first antagonistic pair (m_1 and m_2) simulates the actions of the deltoid anterior and posterior on the shoulder. Therefore, the contraction of muscle m_1, produces shoulder flexion, while the contraction of muscle m_2 produces shoulder extension. The second pair (m_3 and m_4) simulates the actions of the biceps and triceps long on the elbow, flexing and extending the forearm. And finally the third pair (m_5 and m_6) simulates the actions of the wrist flexor and extensor group. The effect and interactions of these muscles with the skeleton can be characterized geometrically and functionally.

The geometry of a single musculotendon unit is detailed in Figure 3. Each musculotendon unit j is of length $l_{mt,j}$, and is composed by a muscle of length $l_{m,j}$ and an infinitely rigid tendon of constant length $l_{t,j}$. The muscle routing is pulley-like. In other words each unit is wrapped around a circumference of constant radius $r_{j,k}$, centered at the axis of rotation of its corresponding degree of freedom q_k. As shown in Figure 3, the origin and insertion points of the muscles are not explicitly defined, instead a joint rest position qr_k and a rest musculotendon length $l_{mtr,j}$ are specified. These reference parameters help to quantify the changes in length or geometry $\Delta l_{mt,j}$ of the unit. An example of such a change in length is featured in the same figure, where an elbow extension motion is performed and the new length of the musculotendon unit is given by the change of arc length with respect to the rest position.

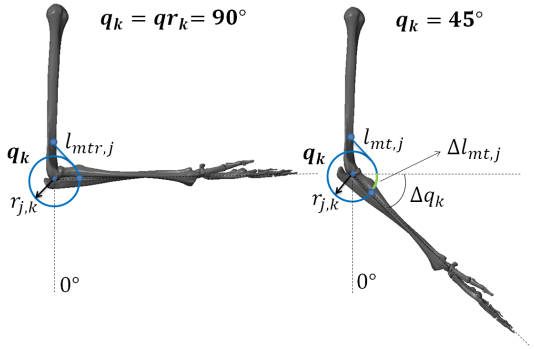

Figure 3: *Musculotendon geometric model*

Therefore, the total length of the musculotendon unit can be mathematically expressed as:

$$l_{mt,j} = l_{mtr,j} - r_{j,k}(q_k - qr_k) \tag{3}$$

$$l_{mt,j} = l_{m,j} + l_{t,j} \tag{4}$$

Where the musculotendon resting length $l_{mtr,j}$ is simply the sum of the muscle rest length $l_{mr,j}$ and constant tendon length $l_{t,j}$:

$$l_{mtr,j} = l_{mr,j} + l_{t,j} \tag{5}$$

Solving equation 4 for $l_{m,j}$ and replacing $l_{mt,j}$ from equation 3, the changes in muscle length $l_{m,j}$ and shortening velocity $\dot{l_{m,j}}$ can be described as follows:

$$l_{m,j} = l_{mtr,j} - r_{j,k}(q_k - qr_k) - l_{t,j} \tag{6}$$

$$\dot{l_{m,j}} = -r_{j,k}\dot{q_k} \tag{7}$$

Each musculotendon unit can apply a force $F_{m,j}$ on a specific degree of freedom, generating a torque that moves the skeletal system. Therefore, the total torque of a set D_k of muscles on the degree of freedom k can be expressed as:

$$\Gamma_k = F_{m,j} r_{j,k}, \quad j \in D_k \tag{8}$$

In order to describe the force generating properties of each muscle the functional Hill muscle model [Hill 1938] was used. As shown

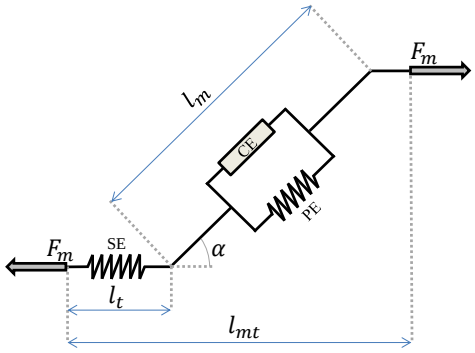

Figure 4: *Musculotendon functional model [Erdemir et al. 2007]*

in figure 4, this model consists of a contractile element CE (non-linear visco-elastic relationship) in parallel with a passive element PE (non-linear spring), and in series with a tendon SE (serial non-linear spring). It is also characterized by a pennation angle α, representing the orientation of the fibers with regard to the tendon. This model has been widely used in biomechanics, and recently within the animation community [Mordatch et al. 2013; Wang et al. 2012], even if the numerous parameters necessary to completely define its behavior are difficult to obtain in vivo. With this model, the muscle force $F_{m,j}$ of a musculotendon unit j can be summarized as the sum of the contractile and passive forces:

$$F_{m,j} = [f_p(\bar{l}_{m,j}) + a_j \cdot f_l(\bar{l}_{m,j}) \cdot f_v(\dot{\bar{l}}_{m,j})] \cdot F_{0,j} \tag{9}$$

Where f_p is the passive force relationship, a_j is the muscle activation, f_l is the force-length relationship, f_v the force-velocity relationship, F_{0j} is the maximum isometric force, and $\bar{l}_{mj}$ the normalized length of the muscle unit. This length is obtained by dividing the muscle length by its optimal fiber length $l_{o,j}$ or the length at which the muscle has its greatest ability to produce force. Several models have been proposed to approximate the f_l, f_v and f_p relationships with regard to experimental data. The chosen models for this work were the approximations (Figure 5) made by [Rengifo et al. 2010].

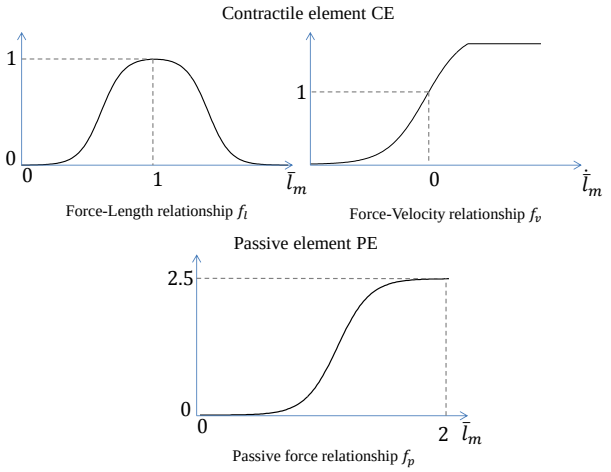

Figure 5: *Force generation capacity of muscles.*

Once the muscle force has been determined, the force at the tendon $f_{t,j}$ can be obtained by simply taking into account the pennation angle of the fibers:

$$f_{t,j} = F_{m,j} \cdot \cos \alpha_j \tag{10}$$

In this study the pennation angles were neglected, and therefore $F_{m,j}$ was directly the output of the musculotendon unit.

Finally, complete dynamics of this unit also includes the activation dynamics, describing the non-linear temporal relationship between the neural excitation and the effective activation of the muscle [Buchanan et al. 2004]. This non-linear relationship can be approximated by a second order differential equation [Venture et al. 2005; Venture et al. 2006], exhibiting different time constants for activation and deactivation:

$$\dot{e}_j = (u_j - e_j)/\tau_{ne}$$

$$\dot{a}_j = \begin{cases} (e_j - a_j)/\tau_{act} & , \quad e_j \geq a_j \\ (e_j - a_j)/\tau_{deact} & , \quad e_j < a_j \end{cases} \tag{11}$$

Where u_j is the neural excitation, a_j the muscle activation, e_j an intermediate variable, τ_{ne} the neural excitation time constant (often neglected), τ_{act} and τ_{deact} the activation and deactivation time constants respectively. In the current work, activation dynamics was taken into account a posteriori as it is shown in section 2.6.

2.4 Synergy driven forward dynamics pipeline

The character model was used within the synergy-driven forward dynamics pipeline in Figure 6. The aim of this pipeline is to replay the recorded human arm motion q^d on a virtual arm by using muscle synergies. Essentially, the pipeline tries to overcome two limitations that prevent a perfect motion reconstruction using the raw synergies: the uncertainty in muscle parameters, and the distinct dynamics of the character model with respect to the real human. This is achieved through two consecutive adaptation stages: a muscle parameter (P) optimization, and a synergy combination coefficient ($C(t)$) optimization and filtering. At each iteration the output of these procedures is used in the conversion from muscles synergies to muscle activations $A(t)$, which finally results in skeletal motion that is used in the evaluation of the optimizations.

2.5 Muscle parameters optimization

Muscle parameters are subject specific and are initially unknown. The estimation of such parameters is important since they affect the mapping from synergies to motion. Therefore, an optimization was designed in order to determine a set of parameters that enhanced this mapping. These parameters were: the maximal forces $F_{o,j}$, moment arms $r_{j,k}$, rest lengths $l_{mr,j}$, and joint rest positions qr_k. The following optimization was repeated for each muscle-actuated degree of freedom q_k with the purpose of finding the parameters P_k of the muscles acting directly on it:

$$\begin{aligned} &\underset{P_k}{\text{minimize}} \quad \sum_{t=0}^{T} (q_k(t) - q_k^d(t))^2 \\ &P_k = [F_{o,j}, l_{mr,j}, r_{j,k}, qr_k], \quad j \in D_k, \quad P_k \in P \end{aligned} \tag{12}$$

$$\text{subject to} = \begin{cases} F_{o,j} > 0 \\ r_{j,k} > 0 \text{ or } r_{j,k} < 0 \text{ (action dependent)} \\ 0.8 < \frac{l_{mr,j}}{lo,j} < 1.2 \\ -180^\circ \leq qr_k \leq 180^\circ \end{cases}$$

Where, T is the total simulation time, D_k is a set containing the muscles acting on joint q_k and P is the set containing the parameters for all joints. The constraints on $r_{j,k}$ are action dependent. In other words the moment arms are positive or negative depending on the sign of their expected actions on the joints. The constraints on $l_{mr,j}$ correspond to known intervals for this value with regard to $l_{o,j}$.

Average initial values for $F_{o,j}$ and $r_{j,k}$ were taken from biomechanical studies [Holzbaur et al. 2005] and each muscle was assigned values corresponding to the real muscle it simulated (section 2.3.2). For the wrist extensor and flexor group, the parameters of the extensor carpi ulnaris and flexor carpi radialis were used. However, certain parameters, such as qr_k and $l_{mr,j}$, had to be arbitrarily chosen since they are specific to the muscle model used.

This, and following optimization problems were solved in MATLAB® via the *fmincon* function and its *interior-point algorithm*. In each optimization, only the degree of freedom of interest was populated with muscles, while the rest of the skeleton was driven kinematically. At each iteration, the entire throw was simulated by driving the arm with the extracted synergies. Then, the global error on joint position was computed, and new muscle parameters were proposed for subsequent iterations until the error was minimized.

2.6 $C(t)$ optimization and filtering

The character model will always be a rough approximation of the real recorded human (with different mass, muscle parameters, muscle routing etc.) Therefore, a part of the control signals (synergies) should be adapted to deal with the distinct dynamics of the model. To address this, while the task independent part of the synergy, synergy matrix W, was kept unmodified, an optimization was implemented to adapt the task dependent part of the synergy, or time-varying combination coefficients $C(t)$, at each time step:

$$\begin{aligned} &\underset{c_i(t-1)}{\text{minimize}} \quad \sum_{k=1}^{ndofs} |q_k(t) - q_k^d(t)| \\ &\text{subject to} \quad 0 < c_i(t-1) < 1, \\ &c_i(t-1) \in C(t-1), \quad i = 1...N \end{aligned} \tag{13}$$

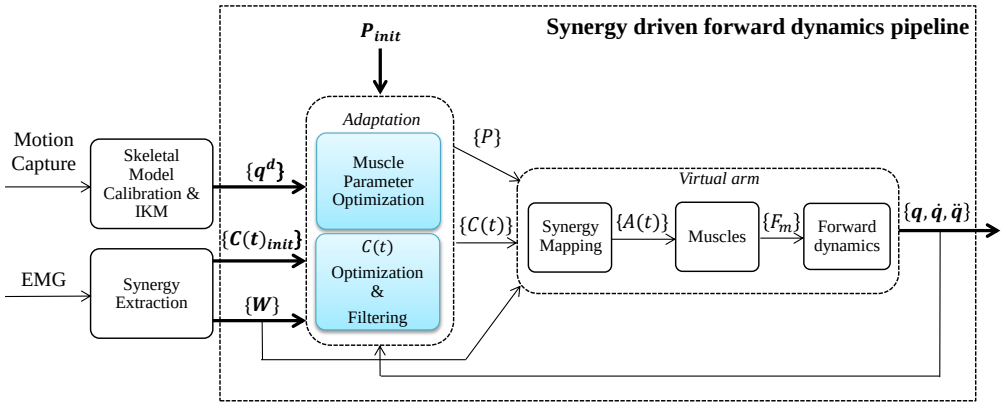

Figure 6: *Synergy driven forward dynamics pipeline*

Where $ndofs$ is the the total number of muscle actuated degrees of freedom in the model (3 in our case), and N is the number of synergies.

The previous optimization routine did not take into account the muscle activation dynamics and often resulted in a apparently noisy signal. In fact, after optimization, the resulting signal was more comparable to a neural excitation than to a real muscular activation due to the lack of dynamical evolution in the muscle model used. We circumvented this issue by applying a second order numerical filter to the optimized signal, representing the activation dynamics, thanks to the model presented in section 2.3.2.
Assuming that the activation and deactivation constant times are equal, and that the relation between $C(t)$ and the activation $A(t)$ is straightforward, equation 11 can be written in the Laplace domain as:

$$\frac{C_i(p)}{U(p)} = \frac{1}{(1+\tau_{act}p)(1+\tau_{ne}p)} \tag{14}$$

Where τ_{act} and τ_{ne} were set to 50ms and 1ms respectively. Next, the z-transform associated to the activation dynamics, can be written as:

$$\frac{C_i(z)}{U(z)} = \frac{b_1 z + b_0}{a_2 z^2 + a_1 z + a_0} \tag{15}$$

With

$$b_1 = \frac{\tau_{ne}(1-e^{-T_e/\tau_{ne}}) - \tau_{act}(1-e^{-T_e/\tau_{act}})}{\tau_{ne}-\tau_{act}}$$

$$b_0 = e^{-T_e/\tau_{ne}} e^{-T_e/\tau_{act}} - \frac{e^{-T_e/\tau_{ne}} - e^{-T_e/\tau_{act}}}{\tau_{act}-\tau_{ne}}$$

$$a_2 = 1$$

$$a_1 = -(e^{-T_e/\tau_{ne}} + e^{-T_e/\tau_{act}})$$

$$a_0 = e^{-T_e/\tau_{ne}} e^{-T_e/\tau_{act}}$$

Equation 15 can then be multiplied by z^{-2} to be only dependent of negative powers of z, and finally, thanks to the delay theorem, we can write the following recursive equation:

$$\begin{aligned} c_i(kT_e) \quad = \quad & -a_1 c_i((k-1)T_e) - a_0 c_i((k-2)T_e) \\ & + b_1 e((k-1)T_e) + b_0 e((k-2)T_e) \end{aligned} \tag{16}$$

The sampling resulted in a static gain equal to $K = \frac{(b_1+b_0)}{(a_2+a_1+a_0)}$, therefore equation 17 was divided by this gain to get a normalized combination coefficient:

$$c_{i_{norm}}(kT_e) = \frac{c_i(kT_e)}{K} \tag{17}$$

3 Results and Discussion

3.1 Synergy extraction results

A set of synergies was obtained thanks to the synergy extraction algorithm described in section 2.2. These synergies capture the relative activation levels of groups of muscles (Figure 7), their intensity and triggering times (Figure 8). Furthermore, as evidenced in [Cruz Ruiz et al. 2015], each synergy recruits groups of muscles with biomechanical actions corresponding to specific motion phases. Figure 8, shows the combination coefficients $C(t)$ containing the time-variations of the synergies for all the concatenated throws. The shape of these coefficients is repeatable across throws, with only small differences in amplitude and time duration.

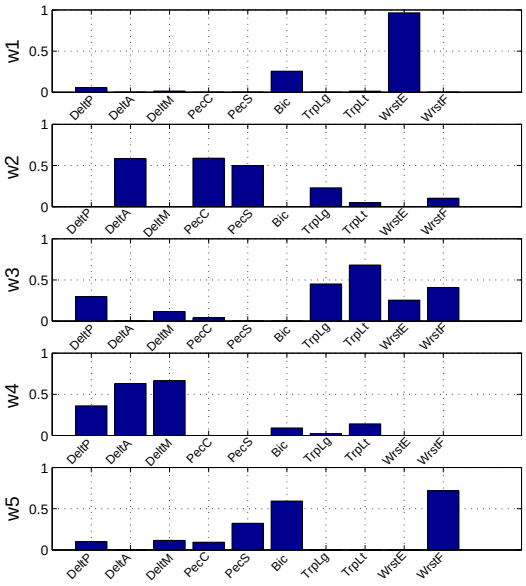

Figure 7: *Extracted synergies* w_i

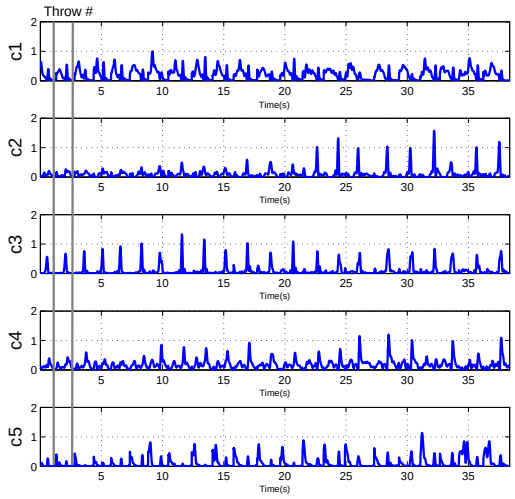

Figure 8: *Extracted time-varying combination coefficients* c_i

For the results featured in the next sections only the part of these signals corresponding to a 2m throw was used.

3.2 Synergy-driven motion with uncertain muscle parameters

Next, the synergies were used to reconstruct the activations to drive muscles m_1 to m_6 in the model, using equation 1. Figure 9 depicts the angular trajectories of the three muscle-driven degrees of freedom and the trajectories obtained from motion capture data. As

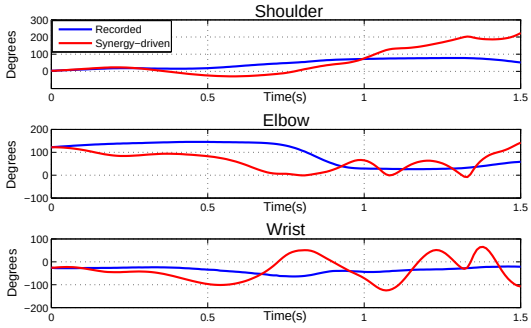

Figure 9: *Synergy-driven motion with uncertain muscle parameters*

expected, the motion did not follow the general trends of the desired joint trajectories. This is due to the fact that the mapping made from synergies to motion was especially hindered by the arbitrary choice of resting angles and lengths, which determine the equilibrium position of the joint. Furthermore, the synergies encode unnecessary information of muscles used during the extraction, but not considered in the character model.

3.3 Synergy-driven motion with optimized muscle parameters

The previous results highlight the fact that a good estimation of muscle parameters is necessary in order to properly evaluate the action of the synergies. Therefore, we applied the optimization in section 2.5 and drove the model with synergies. As shown in Figure 10, compared to the previous section, results are far better and most muscle-driven joint trajectories follow quite correctly the recorded ones (coefficient of determinations: $r^2_{shoulder} = 0.8971, r^2_{elbow} = 0.8904$ and negative for the wrist). The results show that the synergies are able to capture and roughly reproduce general trends in the joint positions. For instance, shoulder flexion gradually increases and then decreases towards the end of the motion. Elbow extension is made halfway through the motion (during the acceleration phase) as the highest wrist extended position is reached. Nevertheless, small variations still remain, and a huge off-hook is visible for the wrist trajectory. We attribute this behavior to the fact that the muscles were not optimized in one sole procedure.

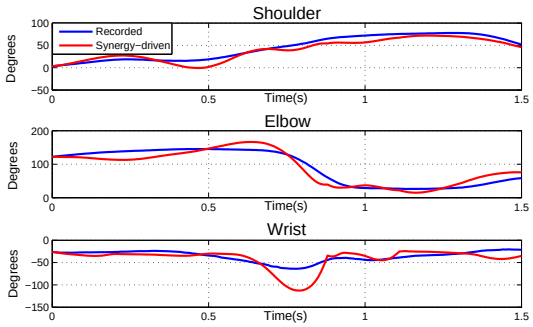

Figure 10: *Synergy-driven motion with optimized muscle parameters*

3.4 Optimized synergy-driven motion

Next, the time-varying combination coefficients $C(t)$ were optimized and filtered as described in section 2.6. This process modulated when and how much each synergy $w_i(t)$ is triggered according to the character model and the desired positions. The coefficients before and after this procedure are featured in Figure 11, while the resulting motion with regard to the record one is featured in Figure 12. The motion is tracked more accurately than with solely implementing a parameter optimization. The coefficient of determination for all degrees of freedom was improved, especially for the wrist ($r^2_{shoulder} = 0.9268, r^2_{elbow} = 0.9420, r^2_{wrist} =$

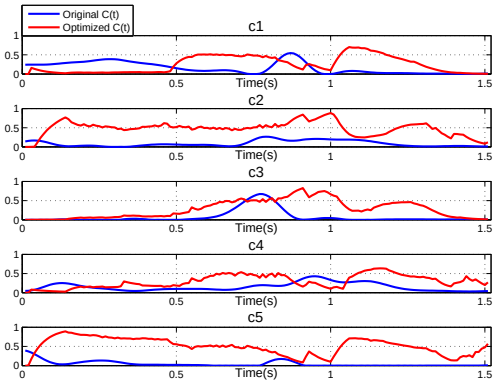

Figure 11: *C(t) before and after optimization and filtering*

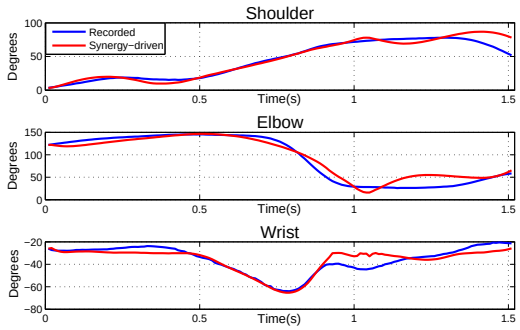

Figure 12: *Motion after C(t) optimization and filtering*

0.8136). An animated version of these results is featured in the accompanying video [1].

The results validate the control strategy we adopted as a relevant direct dynamics motion control strategy. However, $C(t)$ was very affected by the optimization (Figure 11) and resulted in very different muscle activation shapes. We believe this issue did not originate in our estimation of the original $C(t)$ coefficient matrix, which has been validated [Cruz Ruiz et al. 2015]. Its origins lie in a set of limitations that will be discussed in the following section.

3.5 Limitations and perspectives

Although the proposed pipeline reduced the actuation redundancy, and improved the motion reconstruction quality using synergies, several limitations still need to be resolved.
First of all, various simplifications were made on the muscle models which distorted the resulting motion and increased the need for unnecessary adaptations of $C(t)$. These models can be improved by including time-varying moment arms, which will vary the capacity of the muscle to exert torque against the joint positions. Also, by taking into account the activation dynamics inside the optimization scheme, which will lead to smoother motions.

Separate optimizations were made for each muscle-actuated degree of freedom, hindering the overall motion reconstruction quality. Optimizing all parameters in one procedure will guarantee that the dynamical effects among synergy-driven joints are considered simultaneously, yielding a higher motion reconstruction quality. Furthermore, a better muscle parameter estimation (so a better matching of the model with regard to the real human) will lead to fewer modifications in combination coefficients $C(t)$.

The synergies encoded the variability of a larger set of muscles than those that were actually used, hampering the accuracy of reconstruction of muscle activations and kinematics. Recent studies have evidenced, that in fact, the number and choice of muscles impacts the structure of synergies [Steele et al. 2013]. Therefore, the synergy extraction should be made from the relevant muscles only.

Controlling musculoskeletal systems is usually time consuming, with some state of the art approaches needing up to 10h to 12h [Wang et al. 2012] [Geijtenbeek et al. 2013] and several computer cores [Wang et al. 2012] [Lee et al. 2014] to synthesize some seconds of animation. Our framework is also computationally expensive. Although the total parameter optimization time was of 1h, the synergy coefficient optimization was of 12h on an HP Intel(R) Core(TM) i7-3740QM CPU 2.70GHz. Nevertheless, we believe that by addressing the limitations as described above, less modifications will be necessary on the synergy combination coefficients. Additionally, these coefficients could be optimized using multiple objective terms (such as muscle effort and task trajectory tracking [Lee et al. 2014]) which will better constraint the feasible solution space.

Further enhancements will include using synergy models of different orders, and synthesizing new motions by specifying task-space goals (ball release velocity and angle) and synergy adaptation. We also expect to derive rules from the relationships between such goals, and the variations in the combination coefficients $C(t)$ (both raw and optimized), to design more efficient controllers.
Finally, we would like to recall that the framework is able to reproduce throwing motions only. However, a more complete database of synergies could be created and used with respect to standard task-space goals in the future. To start, this database could contain other tasks involving control of one arm, such as writing.

[1] Online version: https://youtu.be/YHO3eeFI0NI

4 Conclusion

The concept of synergies has rarely been exploited within the animation community for generating highly dynamic motions on musculoskeletal characters. State of the art approaches have produced outstanding results [Geijtenbeek et al. 2013] [Wang et al. 2012][Lee et al. 2014], however a large number of control signals need to be computed (usually one per muscle). Moreover, the similarity of such signals with real human data is seldom reported.
This work is a first step in showing the potential of synergies in a forward dynamics strategy, and their use for the dimensionality reduction of a complex control problem. First, the concept of muscle synergies and experimental protocol were introduced. Then, the musculoskeletal model and forward dynamics pipeline were presented. Results showed that the successive optimization of the muscle parameters and the time-varying combination coefficients $C(t)$ of synergies enabled an accurate replay of the motion. This evidences the fact that the muscle synergy approach can be a solution for forward dynamics motion control. Furthermore, it also shows that a reduced set of control signals can be used to drive a larger set of actuators, providing a promising way to drive overactuated models (such as musculoskeletal models) for animation purposes.

Acknowledgements

The authors wish to thank Anthony Sorel and Antoine Muller for their precious work. This study was funded by the ANR project ENTRACTE (Grant agreement: ANR 13-CORD-002-01).

References

ALESSANDRO, C., DELIS, I., NORI, F., PANZERI, S., AND BERRET, B. 2013. Muscle synergies in neuroscience and robotics: from input-space to task-space perspectives. *Frontiers in computational neuroscience 7*.

BUCHANAN, T. S., LOYD, D. G., MANAL, K., AND BESIER, T. F. 2004. Neuromusculoskeletal modeling : Estimation of muscle forces and joints moments and movements from measurements of neural command. *Journal of Applied Biomechanics 20*, 367–395.

CRUZ RUIZ, A. L., PONTONNIER, C., AND DUMONT, G. 2014. A bio-inspired limb controller for avatar animation. *Computer methods in biomechanics and biomedical engineering 17*, sup1, 174–175.

CRUZ RUIZ, A. L., PONTONNIER, C., SOREL, A., AND DUMONT, G. 2015. Identifying representative muscle synergies in overhead football throws. *Computer Methods in Biomechanics and Biomedical Engineering*, 2.

D'AVELLA, A., AND LACQUANITI, F. 2013. Control of reaching movements by muscle synergy combinations. *Frontiers in computational neuroscience 7*.

DE ZEE, M., HANSEN, L., WONG, C., RASMUSSEN, J., AND SIMONSEN, E. B. 2007. A generic detailed rigid-body lumbar spine model. *Journal of biomechanics 40*, 6, 1219–1227.

DUMAS, R., CHEZE, L., AND VERRIEST, J.-P. 2007. Adjustments to mcconville et al. and young et al. body segment inertial parameters. *Journal of biomechanics 40*, 3, 543–553.

ERDEMIR, A., MCLEAN, S., HERZOG, W., AND VAN DEN BOGERT, A. J. 2007. Model-based estimation of muscle forces exerted during movements. *Clinical Biomechanics 22*, 2, 131–154.

GEIJTENBEEK, T., AND PRONOST, N. 2012. Interactive character animation using simulated physics: A state-of-the-art review. *Comput. Graph. Forum 31*, 8 (Dec.), 2492–2515.

GEIJTENBEEK, T., VAN DE PANNE, M., AND VAN DER STAPPEN, A. F. 2013. Flexible muscle-based locomotion for bipedal creatures. *ACM Trans. Graph. 32*, 6 (Nov.), 206:1–206:11.

GERRITSEN, K. G., VAN DEN BOGERT, A. J., AND NIGG, B. M. 1995. Direct dynamics simulation of the impact phase in heel-toe running. *Journal of biomechanics 28*, 6, 661–668.

GEYER, H., AND HERR, H. 2010. A muscle-reflex model that encodes principles of legged mechanics produces human walking dynamics and muscle activities. *IEEE Transactions on Neural Systems and Rehabilitation Engineering 18*, 3 (June), 263–273.

HERMENS, H. J., FRERIKS, B., MERLETTI, R., STEGEMAN, D., BLOK, J., RAU, G., DISSELHORST-KLUG, C., AND HÄGG, G. 1999. European recommendations for surface electromyography. *Roessingh Research and Development 8*, 2, 13–54.

HILL, A. V. 1938. The Heat of Shortening and the Dynamic Constants of Muscle. *Royal Society of London Proceedings Series B 126*, 136–195.

HODGINS, J., AND WOOTEN, W. 1998. Animating human athletes. In *Robotics Research*. Springer London, 356–367.

HOLZBAUR, K. R., MURRAY, W. M., AND DELP, S. L. 2005. A model of the upper extremity for simulating musculoskeletal surgery and analyzing neuromuscular control. *Annals of biomedical engineering 33*, 6, 829–840.

HORSMAN, M. K., KOOPMAN, H., VAN DER HELM, F., PROSÉ, L. P., AND VEEGER, H. 2007. Morphological muscle and joint parameters for musculoskeletal modelling of the lower extremity. *Clinical biomechanics 22*, 2, 239–247.

KIM, H., AND PARK, H. 2008. Nonnegative matrix factorization based on alternating nonnegativity constrained least squares and active set method. *SIAM Journal on Matrix Analysis and Applications 30*, 2, 713–730.

KONRAD, P. 2005. The abc of emg: A practical introduction to kinesiological electromyography. version 1.0, noraxon inc.

KULPA, R., MULTON, F., AND ARNALDI, B. 2005. Morphology-independent representation of motions for interactive human-like animation. *Computer Graphics Forum 24*, 3, 343–351.

LEE, Y., PARK, M. S., KWON, T., AND LEE, J. 2014. Locomotion control for many-muscle humanoids. *ACM Trans. Graph. 33*, 6 (Nov.), 218:1–218:11.

MORDATCH, I., WANG, J. M., TODOROV, E., AND KOLTUN, V. 2013. Animating human lower limbs using contact-invariant optimization. *ACM Trans. Graph. 32*, 6 (Nov.), 203:1–203:8.

MULLER, A., GERMAIN, C., PONTONNIER, C., AND DUMONT, G. 2015. A simple method to calibrate kinematical invariants: Application to overhead throwing. In *33rd International Conference on Biomechanics in Sports (ISBS 2015)*.

MULLER, A., PONTONNIER, C., GERMAIN, C., AND DUMONT, G. 2015. Dealing with modularity of multibody models. *Computer methods in biomechanics and biomedical engineering*, 2.

PRONOST, N., AND DUMONT, G. 2007. Dynamics-based analysis and synthesis of human locomotion. *The Visual Computer 23*, 7, 513–522.

RENGIFO, C., AOUSTIN, Y., PLESTAN, F., AND CHEVALLEREAU, C. 2010. Distribution of forces between synergistics and antagonistics muscles using an optimization criterion depending on muscle contraction behavior. *Journal of biomechanical engineering 132*, 4.

SI, W., LEE, S.-H., SIFAKIS, E., AND TERZOPOULOS, D. 2014. Realistic biomechanical simulation and control of human swimming. *ACM Trans. Graph. 34*, 1 (Dec.), 10:1–10:15.

STEELE, K. M., TRESCH, M. C., AND PERREAULT, E. J. 2013. The number and choice of muscles impact the results of muscle synergy analyses. *Frontiers in Computational Neuroscience 7*, 105.

VENTURE, G., YAMANE, K., AND NAKAMURA, Y. 2005. Identifying musculo-tendon parameters of human body based on the musculo-skeletal dynamics computation and hill-stroeve muscle model. In *2005 5th IEEE-RAS International Conference on Humanoid Robots*, 351–356.

VENTURE, G., YAMANE, K., AND NAKAMURA, Y. 2006. Application of non-linear least square method to estimate the muscle dynamics of the elbow joint. In *IFAC - Int. Conf. on System Identification*, 1168–1173.

VICOVARO, M., HOYET, L., BURIGANA, L., AND O'SULLIVAN, C. 2014. Perceptual evaluation of motion editing for realistic throwing animations. *ACM Trans. Appl. Percept. 11*, 2 (June), 10:1–10:23.

WANG, J. M., HAMNER, S. R., DELP, S. L., AND KOLTUN, V. 2012. Optimizing locomotion controllers using biologically-based actuators and objectives. *ACM Trans. Graph. 31*, 4 (July), 25:1–25:11.

WILLIGENBURG, N. W., DAFFERTSHOFER, A., KINGMA, I., AND VAN DIEËN, J. H. 2012. Removing ecg contamination from emg recordings: A comparison of ica-based and other filtering procedures. *Journal of electromyography and kinesiology 22*, 3, 485–493.

YIN, K., LOKEN, K., AND VAN DE PANNE, M. 2007. Simbicon: Simple biped locomotion control. *ACM Trans. Graph. 26*, 3 (July).